Chinese Journal of Aeronautics, (2014),27(1): 169–181

Chinese Society of Aeronautics and Astronautics
& Beihang University

Chinese Journal of Aeronautics

cja@buaa.edu.cn
www.sciencedirect.com

Theoretical study of flow ripple for an aviation axial-piston pump with damping holes in the valve plate

Guan Changbin [a,b], **Jiao Zongxia** [a,c,*], **He Shouzhan** [a,c]

[a] *School of Automation Science and Engineering, Beihang University, Beijing 100191, China*
[b] *Beijing Institute of Control Engineering, Beijing 100080, China*
[c] *Science and Technology on Aircraft Control Laboratory, Beihang University, Beijing 100191, China*

Received 16 January 2013; revised 18 February 2013; accepted 19 March 2013
Available online 2 August 2013

KEYWORDS

Axial-piston pump;
Damping hole;
Flow ripple;
Mathematical models;
Simulation;
Swash plate

Abstract Based on the structure of a certain type of aviation axial-piston pump's valve plate which adopts a pre-pressurization fluid path (consisting a damping hole, a buffer chamber, and an orifice) to reduce flow ripple, a single-piston model of the aviation axial-piston pump is presented. This single-piston model comprehensively considers fluid compressibility, orifice restriction effect, fluid resistance in the capillary tube, and the leakage flow. Besides, the instantaneous discharge areas used in the single-piston model have been calculated in detail. Based on the single-piston model, a multi-piston pump model has been established according to the simple hydraulic circuit. The single- and multi-piston pump models have been realized by the S-function in Matlab/Simulink. The developed multi-piston pump model has been validated by being compared with the numerical result by computational fluid dynamic (CFD). The effects of the pre-pressurization fluid path on the flow ripple and the instantaneous pressure in the piston chamber have been studied and optimized design recommendations for the aviation axial-piston pump have been given out.

1. Introduction

Axial-piston pumps are widely used in aircraft hydraulic systems for supplying hydraulic power to flight actuators because they have high output pressure, high efficiency, and high reliability. However, axial-piston pumps will generate large flow ripple because of their inherent structures and working principles. Flow ripple can induce pressure fluctuation and piping vibration, which are very harmful to aircraft hydraulic systems.[1] According to statistics, almost half of the reported failures of hydraulic systems on aircrafts were due to the fracture of hydraulic pipes.[2] Consequently, the flow ripple of aviation axial-piston pumps is the root cause of hydraulic pipes' fracture. The key component that controls the dynamics of a pump is the valve plate,[3] and the most common measure used to reduce flow ripple is setting up a pressure relief groove or damping hole on the face of the valve plate prior to the opening of a discharge kidney slot reducing severity of the cylinder reverse flow.[4,5] The effect of the pressure relief groove or damping hole on the flow ripple of an axial-piston pump has been a research hotspot.

* Corresponding author. Tel.: +86 10 82338938.
E-mail addresses: guanchangbin@163.com (C. Guan), zxjiao@buaa.edu.cn (Z. Jiao), heshouzhan@126.com (S. He).

Peer review under responsibility of Editorial Committee of CJA.

Production and hosting by Elsevier

1000-9361 © 2014 Production and hosting by Elsevier Ltd. on behalf of CSAA & BUAA. Open access under CC BY-NC-ND license.
http://dx.doi.org/10.1016/j.cja.2013.07.044

Nomenclature

Parameters	Definition
A_h	Section area of the damping hole (m^2)
A_o	Cross section area of the orifice (m^2)
A_p	Cross section area of piston (m^2)
A_v	Discharge orifice area of the throttle valve (m^2)
A_{kd}	Discharge area of the ith piston kidney port in communication with the discharge port (m^2)
A_{kh}	Discharge area of the ith piston kidney port in communication with the damping hole (m^2)
C_d	Discharge coefficient of piston kidney port
C_h	Discharge coefficient of damping hole
C_o	Discharge coefficient of the orifice
C_v	Discharge coefficient of the throttle valve
d_d	Diameter of the piston leakage hole (m)
d_h	Diameter of the damping hole (m)
d_o	Diameter of the orifice (m)
d_p	Piston diameter (m)
dV	Volume change of the piston chamber (m^3)
E	Fluid bulk modulus (Pa)
K_{ih}	Inertia effect factor of the fluid in damping hole
l_k	Length of linearized kidney port (m)
l_p	Total length of the piston (m)
l_{cp}	Instantaneous overlap length of the piston and the cylinder block (m)
l_{h1}, l_{h2}	Lengths of the damping hole (m)
l_{cp0}	Initial overlap length of the piston and the cylinder block when the piston is at TDC (m)
n	Rotation speed of pump (r/min)
P_c	Pressure inside the pump shell chamber (Pa)
P_d	Pressure in discharge port (Pa)
P_T	Pressure of the oil tank (Pa)
P_{bc}	Pressure in buffer chamber (Pa)
P_{pi}	Instantaneous pressure in the ith piston chamber (Pa)
Q_d	Inverse flow rate from discharge port to piston chamber (m^3/s)
Q_g	Geometry flow rate of single piston (m^3/s)
Q_h	Inverse flow rate from damping hole to piston chamber (m^3/s)
Q_l	Leakage flow rate of single piston (m^3/s)
Q_o	Flow rate through the orifice (m^3/s)
Q_p	Total discharge flow rate of axial-piston pump (m^3/s)
Q_v	Flow rate through the throttle valve (m^3/s)
Q_{lv}	Leakage flow rate through the gap between the valve plate and the cylinder block (m^3/s)
Q_{pi}	Discharge flow rate of individual piston to discharge port (m^3/s)
Q_{lci}	Leakage flow rate through the gap between the piston and the cylinder block (m^3/s)
Q_{lsi}	Leakage flow rate through the gap between the swash plate and the slipper (m^3/s)
R	Piston distribution radius (m)
R_1	Inside radius of the inside valve plate seal ring (m)
R_2	Outside radius of the inside valve plate seal ring (m)
R_3	Inside radius of the outside valve plate seal ring (m)
R_4	Outside radius of the outside valve plate seal ring (m)
R_s	Outer radius of the slipper (m)
r_h	Radius of the damping hole (m)
r_k	Width radius of kidney port and discharge port (m)
r_s	Inner radius of the slipper (m)
t	Time (s)
V_0	Initial volume of piston chamber when piston is at TDC (m^3)
V_h	Volume of the damping hole (m^3)
V_{bc}	Volume of the buffer chamber (m^3)
V_{dc}	Discharge chamber control volume (m^3)
V_{pc}	Instantaneous volume of the piston chamber (m^3)
Z	Number of pistons
α_1, α_2, α_3, α_4	Angular segmentation points of calculating A_{kh} (°)
β_1, β_2, β_3, β_4, β_5	Angular segmentation points of calculating A_{kd} (°)
γ	Angle of the swash plate (°)
θ_1, θ_2, θ_3, θ_4, θ_5	Angles used in calculation of the discharge area (°)
φ	Position angle of piston (°)
ω	Angular velocity of pump (rad/s)
ρ	Fluid density (kg/m^3)
μ	Kinetic viscosity of the fluid (m^2/s)
δ_p	Oil film thickness between the piston and the cylinder block (m)
δ_s	Clearance between the slipper and the swash plate (m)
δ_v	Clearance between the valve plate and the cylinder block (m)
Γ_h	Integral area function used to describe the fluid inertia (m^{-1})

Within the last forty years, significant research on cylinder pressure transient and flow ripple of axial-piston pumps has appeared in the literatures. However, almost all the literatures focused on axial-piston pumps with silencing grooves in valve plates. Helgestad et al[6] gave out a method for calculating cylinder pressure in axial-piston hydraulic pumps with or without silencing grooves considering fluid compressibility, cylinder leakage, and orifice restriction effect. Edge and Darling[7,8] put forward an improved theoretical model for cylinder pressure taking fluid inertia in silencing grooves into consideration. Base on the theory of Edge and Darling, Harrison and Edge[9] calculated the total delivery flow ripple of an axial-piston pump with ripple-reduction mechanism by summation of each cylinder flow whose phase difference was considered, but cylinder leakage was neglected in their study. Based on the idealized pump flow model, Manring[10] investigated the actual flow ripple of an axial-piston swash-plate type hydrostatic pump with silencing grooves in its valve plate by considering pump leakage and fluid compressibility. Design aspects of valve plates of slot geometries and their effects on pump volumetric

efficiencies have been analyzed later by him.[11,12] Zhang[13] proposed a new open-loop, reduced order model for the swash plate dynamics of an axial-piston pump with silencing grooves in its valve plate. In Refs. [10–13], pump leakage was just modeled as a laminar flow which was proportional to cylinder pressure and the fluid inertia in silencing grooves was not considered. Refs. [14–17] developed the mathematical model of delivery flow of an axial-piston pump with conical cylinder blocks and investigated the effect of a silencing groove on the flow characteristics of the pump. Li[18] established a single-cylinder flow model of an axial-piston pump with a silencing groove in its valve plate considering fluid compressibility and cylinder leakage. In the single-cylinder flow model, the discharge area was calculated in detail. By summating all cylinder flows communicating with the discharge port, the total flow rate model was derived. The pressure ripple was also calculated by applying the total flow rate model to a simple hydraulic circuit. Ma et al.[19] presented an improved single-cylinder and multi-cylinder pumping dynamics model by studying cylinder leakage flows very carefully and considering the fluid inertia of the timing grooves. Mandal et al.[20] developed a mathematical model of axial-piston pumps that put special emphasis on analyzing the effect of volume variation of the silencing grooves. In Mandal's model, the silencing grooves were seen as a separated control volume where fluid is compressible. Bergada et al[21] developed a comprehensive leakage model for an axial-piston pump which had a timing groove on the valve plate. Based on the proposed leakage model, he presented a single-cylinder and multi-cylinder pump model, and investigated the pressure/flow pump dynamic characteristics.

Although a lot of work has been done to investigate the flow characteristics of axial-piston pumps with silencing grooves in valve plates as mentioned above, only a little effort has been given to theoretical modeling of flow ripple of axial-piston pumps with damping holes. Ma[4] and Qiu[5] investigated the cylinder pressure transient and single-piston flow characteristics of axial-piston pumps with damping holes in valve plates. However, Ma's model and Qiu's model are both not comprehensive because cylinder leakage and detailed change processing of the instantaneous discharge area were not taken into consideration. Besides, they did not consider the pre-pressurization fluid path from the piston chamber to the discharge port, but just regarded the damping hole as a two-dimensional hole.

In this paper, the flow ripple of a certain type of aviation axial-piston pump whose valve plate adopts a damping hole to reduce flow ripple is studied. Based on the detailed analysis on the structure of the aviation axial-piston pump's valve plate, a comprehensive single-piston model is established by modeling the pre-pressurization fluid path from the piston chamber to the discharge port which consists of a damping hole, a buffer chamber, and an orifice. The presented single-piston model considers fluid compressibility, orifice restriction effect, fluid resistance in the capillary tube, and the leakage flow. In addition, the instantaneous discharge areas which are used in the single-piston model are calculated according to their transient change processing. Based on the single-piston model, a multi-piston model for the aviation axial-piston pump is established according to the simple hydraulic circuit. The single- and multi-piston pump models are both realized by Matlab/Simulink frame. In order to validate the developed multi-piston pump model, the computational fluid dynamic (CFD) technology is used to study the flow ripple of the aviation axial-piston pump. The effects of the pre-pressurization fluid path on the flow ripple and the instantaneous pressure in the piston chamber have been discussed.

Section 2 describes the physical system of the aviation axial-piston pump with a damping hole in the valve plate; In Section 3, the single- and multi-piston pump models for the aviation axial-piston pump are developed; Section 4 introduces the computational technique which realizes the developed pump models; Section 5 validates the developed multi-piston pump model by comparing it with the numerical result by CFD and discusses the effect of the pre-pressurization fluid path on the pumping dynamics characteristics. The study is concluded with final remarks in Section 6.

2. Description of the physical system

The pump under consideration is an aviation axial-piston swash-plate type with damping holes in the valve plate as shown in Fig. 1. The pump has nine pistons ($Z = 9$). It is assumed that the pump operation begins when one piston is at the zero reference line (ZRL), as shown in Fig. 1. This position of the piston is called the 'top dead center' (TDC) where the fluid of the piston chamber begins to be compressed. When the cylinder block rotates clockwise, the piston moves within the cylinder towards the valve plate and discharges the fluid in the piston chamber

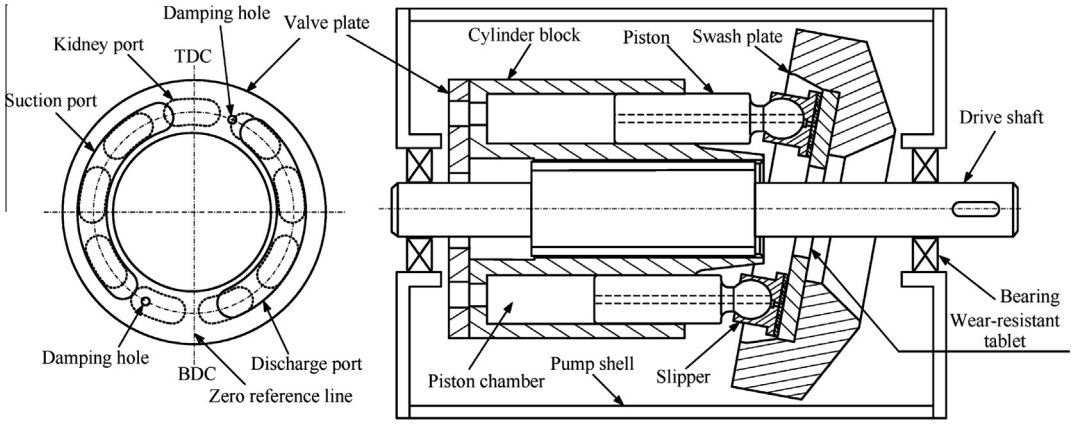

Fig. 1 Schematic of the aviation axial-piston pump.

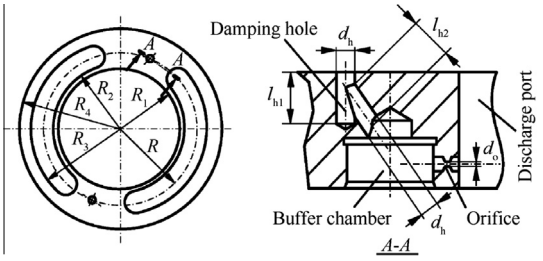

(a) Cutaway view of the damping hole on discharge side

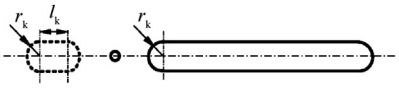

(b) Linearized geometry of kidney port and discharge port

Fig. 2 Schematic of the aviation axial-piston pump's valve plate.

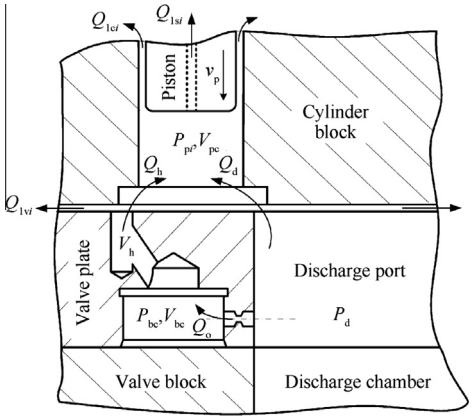

Fig. 3 Single-piston chamber schematic of the aviation axial-piston pump.

to the discharge port. Before communicating with the discharge port, the piston chamber communicates with the damping hole on the discharge side firstly which connects with high-pressure oil and provides pre-pressurization for the fluid in the piston chamber. This discharge continues until the piston reaches the other extreme end, known as the 'bottom dead center' (BDC). Then the piston begins to move toward the swash plate and the fluid rushes into the piston chamber through the suction port. Similarly before communicating with the suction port, the piston chamber communicates with the damping hole on the suction side firstly which connects with low-pressure oil and provides pre-depressurization for the fluid in the piston chamber. The suction process continues until the piston reaches the TDC again. The discharge and suction processes define one completed pumping cycle for one piston.

The total delivery flow is the sum of each individual piston flow communicating with the discharge port over one cycle considering the phase delay between pistons. The present study only focuses on the first half cycle (from the TDC to the BDC) because the pump generates delivery flow only when the piston kidney port communicates with the discharge port.

Fig. 2(a) shows the cutaway view of the damping hole on the discharge side. As shown in Fig. 2(a), the damping hole on the discharge side does not communicate with the discharge port directly. Instead, the damping hole communicates directly with a buffer chamber which is closed by the valve block (as shown in Fig. 1) and then the buffer chamber communicates with the discharge port through an orifice. The damping hole, the buffer chamber, and the orifice constitute a pre-pressurization fluid path which provides a pre-pressurization process for the fluid in the piston chamber to reduce the pressure surge which is the main factor of flow ripple in axial-piston pumps.

3. Mathematical model

3.1. Single-piston model of the aviation axial-piston pump

3.1.1. Instantaneous pressure in the piston chamber

Fig. 3 shows the aviation axial-piston pump's single-piston chamber which is the control fluid volume of the study. As shown in Fig. 3, there are four elements resulting in the variation of the control volume: the geometry flow Q_g brought by motion of the piston, the inverse flow Q_d from the discharge port to the piston chamber, the inverse flow Q_h from the damping hole to the piston chamber, and the leakage flow $Q_l = Q_{lci} + Q_{lsi}$. Q_{lci} is the leakage flow through the gap between the piston and the cylinder block and Q_{lsi} is the leakage flow through the gap between the swash plate and the slipper. Besides, Q_{lvi} is the leakage flow through the gap between the valve plate and the cylinder block and can only be considered in the multi-piston pump model because it is the effect of multiple pistons connecting with the discharge port.[19] The modeling of the three types of leakage flows will be illustrated in Section 3.1.3.

The pressure-rise-rate equation for the control volume can be derived based on the definition of the fluid bulk modulus, which can be expressed as

$$\frac{\mathrm{d}P_{pi}}{\mathrm{d}t} = -\frac{E}{V_{pc}}\frac{\mathrm{d}V}{\mathrm{d}t} \tag{1}$$

where P_{pi} is the instantaneous pressure in the ith piston chamber, t is the time, E is the fluid bulk modulus, $\mathrm{d}V$ is the volume change of the piston chamber, and V_{pc} is the instantaneous volume of the piston chamber which can be given by

$$V_{pc} = V_0 - A_p(1 - \cos\varphi)R\tan\gamma \tag{2}$$

where V_0 is the initial volume of the piston chamber when the piston is at the TDC, $A_p = \pi d_p^2/4$ is the cross section area of the piston, d_p is the diameter of the piston, φ is the position angle of the piston, R is the piston distribution radius, and γ is the angle of the swash plate.

In view of the four elements resulting in the variation of the control volume as shown in Fig. 3, Eq. (1)can be rewritten as

$$\frac{\mathrm{d}P_{pi}}{\mathrm{d}t} = \frac{E}{V_{pc}}(Q_g + Q_d + Q_h - Q_l). \tag{3}$$

The geometry flow Q_g which is determined by the kinematics of the piston can be expressed by

$$Q_g = A_p\omega R t g\gamma \sin\varphi \tag{4}$$

where $\omega = n\pi/30$ is the angular velocity of the pump, and n is the rotation speed of the pump.

The inverse flow Q_d from the discharge port to the piston chamber is modeled using the classical orifice equation, which is described as

$$Q_{\mathrm{d}} = \mathrm{sign}(P_{\mathrm{d}} - P_{\mathrm{p}i}) C_{\mathrm{d}} A_{\mathrm{kd}} \sqrt{\frac{2|P_{\mathrm{d}} - P_{\mathrm{p}i}|}{\rho}} \tag{5}$$

where P_{d} is the pressure in the discharge port, C_{d} and A_{kd} are the discharge coefficient and the instantaneous discharge area of the orifice formed by the intersection of the ith piston kidney port and the discharge port, respectively, and ρ is the fluid density.

With reference to Fig. 3, the continuity equation in the buffer chamber can be given by

$$\frac{\mathrm{d}P_{\mathrm{bc}}}{\mathrm{d}t} = \frac{E}{V_{\mathrm{bc}}}(Q_{\mathrm{o}} - Q_{\mathrm{h}}) \tag{6}$$

where V_{bc} is the volume of the buffer chamber, and Q_{o} is the flow rate through the orifice between the buffer chamber and the discharge port as shown in Fig. 2(a).

The flow rate through the orifice can be obtained by the classic orifice equation, which is expressed as

$$Q_{\mathrm{o}} = \mathrm{sign}(P_{\mathrm{d}} - P_{\mathrm{bc}}) C_{\mathrm{o}} A_{\mathrm{o}} \sqrt{\frac{2|P_{\mathrm{d}} - P_{\mathrm{cb}}|}{\rho}} \tag{7}$$

where C_{o} is the discharge coefficient of the orifice, $A_{\mathrm{o}} = \pi {d_{\mathrm{o}}}^2/4$ is the cross section area of the orifice, and d_{o} is the diameter of the orifice.

According to Fig. 3, the discharge flow of an individual piston to the discharge port consists of two parts: Q_{d} and Q_{o}, which can be expressed as

$$Q_{\mathrm{p}i} = -(Q_{\mathrm{d}} + Q_{\mathrm{o}}). \tag{8}$$

3.1.2. Calculation of the instantaneous discharge areas

The flow rates Q_{d} and Q_{h} described by Eqs. (5) and (14) strongly depend on the respectively instantaneous discharge areas A_{kd} and A_{kh}. The two discharge areas both depend on the position angle φ of the kidney port relative to zero reference line (ZRL). A geometrical calculation for A_{kd} and A_{kh} is carried out for different angular segments when the kidney port locates on the discharge side from the TDC to the BDC ($0 \leqslant \varphi \leqslant 180$). The graphical representation of areas variation with φ is illustrated in Fig. 4.

As shown in Fig. 4(a), the discharge area A_{kh} can be modeled at five angular segments. The derivation of A_{kh} at $[\alpha_1, \alpha_2]$and $[\alpha_3, \alpha_4]$ is given out in Appendix A. Thus the piecewise function of A_{kh} can be derived as

$$A_{\mathrm{kh}} = \begin{cases} 0 & 0 \leqslant \varphi \leqslant \alpha_1 \\ r_{\mathrm{h}}^2\left(\theta_1 - \frac{1}{2}\sin(2\theta_1)\right) + r_{\mathrm{k}}^2\left(\theta_2 - \frac{1}{2}\sin(2\theta_2)\right) & \alpha_1 \leqslant \varphi \leqslant \alpha_2 \\ \pi r_{\mathrm{h}}^2 & \alpha_2 \leqslant \varphi \leqslant \alpha_3 \\ r_{\mathrm{h}}^2\left(\theta_3 - \frac{1}{2}\sin(2\theta_3)\right) + r_{\mathrm{k}}^2\left(\theta_4 - \frac{1}{2}\sin(2\theta_4)\right) & \alpha_3 \leqslant \varphi \leqslant \alpha_4 \\ 0 & \alpha_4 \leqslant \varphi \leqslant \beta_5 \end{cases} \tag{9}$$

where $r_{\mathrm{h}} = d_{\mathrm{h}}/2$ is the radius of the damping hole, r_{k} is the width radius of the kidney port and the discharge port as shown in Fig. 2(b). θ_1, θ_2, θ_3, and θ_4 are given in Eqs. (A11), (A12), (B2), and (B3).

Similarly, the discharge area A_{kd} can also be modeled at five angular segments ($[0, \beta_1]$, $[\beta_1, \beta_2]$, $[\beta_2, \beta_3]$, $[\beta_3, \beta_4]$ and $[\beta_4, \beta_5]$) according to Fig. 4(a). The expression of A_{kd} at $[\beta_1, \beta_2]$ is derived in Appendix A, and the models of A_{kd} at other segments can be obtained easily. Therefore, the piecewise function of A_{kd} can be described as

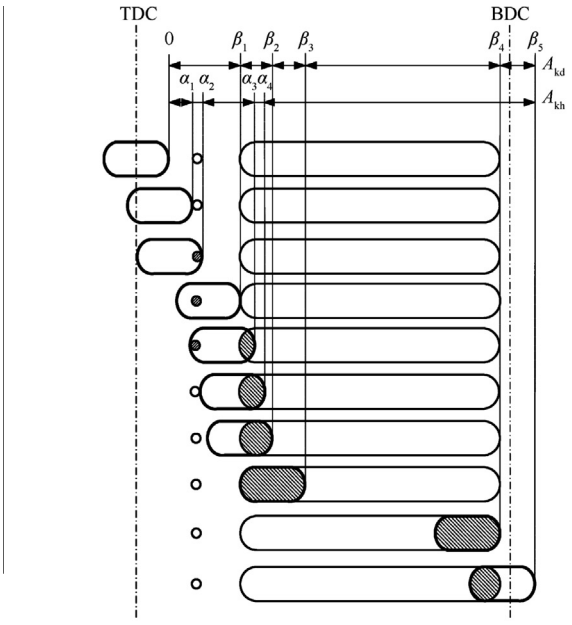

(a) Graphical representation of instantaneous discharge areas variation

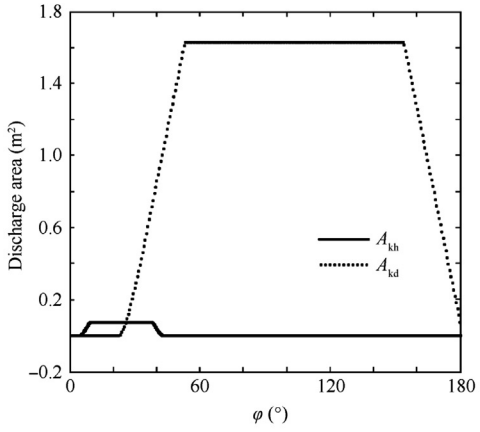

(b) Instantaneous discharge areas

Fig. 4 Calculation of the instantaneous discharge areas.

$$A_{\mathrm{kd}} = \begin{cases} 0 & 0 \leqslant \varphi \leqslant \beta_1 \\ r_{\mathrm{k}}^2(2\theta_5 - \sin(2\theta_5)) & \beta_1 \leqslant \varphi \leqslant \beta_2 \\ \pi r_{\mathrm{k}}^2 + 2r_{\mathrm{k}}(\varphi - \beta_2)R & \beta_2 \leqslant \varphi \leqslant \beta_3 \\ 2r_{\mathrm{k}} l_{\mathrm{k}} + \pi r_{\mathrm{k}}^2 & \beta_3 \leqslant \varphi \leqslant \beta_4 \\ 2r_{\mathrm{k}}[l_{\mathrm{k}} - (\varphi - \beta_4)R] + \pi r_{\mathrm{k}}^2 & \beta_4 \leqslant \varphi \leqslant \beta_5 \end{cases} \tag{10}$$

where l_{k} is the length of the linearized kidney port as shown in Fig. 2(b), and θ_5 is given in Eq. (C2).

The calculation of the instantaneous discharge areas of the axial-piston pump in the present study is carried out using Eqs. (9) and (10). The calculation results are shown in Fig. 4(b).

3.1.3. Modeling of the inverse flow from the damping hole

Referring to Figs. 3 and 4(a), Q_{h} can be modeled at three segments according to its different flow path.

When the angle of rotation φ is at $[0, \alpha_1]$ and $[\alpha_4, \beta_5]$, Q_h can be expressed as

$$Q_h = 0 \tag{11}$$

when φ is at $[\alpha_2, \alpha_3]$, the damping hole is completely included in the kidney port, and the flow path of Q_h is the damping hole, which can be regarded as a capillary tube because $(l_{h1} + l_{h2})/d_h > 4$ (d_h, l_{h1}, and l_{h2} are the diameter and lengths of the damping hole as shown in Fig. 2(a)). Therefore, Q_h is given by

$$Q_h = \frac{\pi d_h^4 (P_{bc} - P_{pi})}{128\mu(l_{h1} + l_{h2})} \tag{12}$$

where P_{bc} is the pressure in the buffer chamber and μ is the dynamic viscosity of the fluid.

When φ is at $[\alpha_1, \alpha_2]$ and $[\alpha_3, \alpha_4]$, the flow path of Q_h is the concatenation of the damping hole and the orifice A_{kh}. Thus the pressure difference between the piston chamber and the discharge port consists of two terms: an orifice term and a capillary resistance term. The pressure drop can be given by

$$|P_{bc} - P_{pi}| = \frac{\rho}{2}\left(\frac{Q_h}{C_h A_{kh}}\right)^2 + \frac{128\mu(l_{h1} + l_{h2})Q_h}{\pi d_h^4} \tag{13}$$

where C_h and A_{kh} are the discharge coefficient and the variable discharge area of the orifice formed by the intersection of the ith piston kidney port and the damping hole.

Q_h can be calculated as the root of Eq. (13) which can be seen as a unary quadratic equation. Therefore Q_h can be written as

$$Q_h = \text{sign}(P_{bc} - P_{pi})\frac{-b + \sqrt{b^2 - 4ac}}{2a} \tag{14}$$

where

$$\begin{cases} a = \frac{\rho}{2C_h^2 A_{kh}^2} \\ b = \frac{128\mu(l_{h1}+l_{h2})}{\pi d_h^4} \\ c = -|P_{bc} - P_{pi}|. \end{cases} \tag{15}$$

Thus, the piecewise function of Q_h can be described as

$$Q_h = \begin{cases} 0 & 0 \leqslant \varphi \leqslant \alpha_1 \ \& \ \alpha_4 \leqslant \varphi \leqslant \beta_5 \\ \text{sign}(P_{bc} - P_p i)\frac{-b+\sqrt{b^2-4ac}}{2a} & \alpha_1 \leqslant \varphi \leqslant \alpha_2 \ \& \ \alpha_3 \leqslant \varphi \leqslant \alpha_4 \\ \frac{\pi d_h^4 (P_{bc} - P_{pi})}{128\mu(l_{h1}+l_{h2})} & \alpha_2 \leqslant \varphi \leqslant \alpha_3 \end{cases} \tag{16}$$

3.1.4. Leakage flows

As shown in Fig. 5, in addition to the flow through the discharge port and the damping hole, certain leakage flows take place in the pump which help lubricating parts with relative motions. As mentioned previously, there are three types of leakage flows in the axial-piston pump: Q_{lci}, Q_{lsi}, and Q_{lv}. The three types of leakage flows were modeled by Jaroslav and Monika.[22]

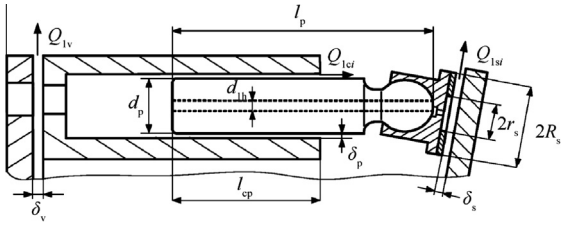

Fig. 5 Schematic diagram of piston leakage modeling.

With reference to Fig. 5, the leakage flow through the clearance between the piston and the cylinder block can be expressed as

$$Q_{lci} = \frac{\pi d_p \delta_p^3}{12\mu l_{cp}}(P_{pi} - P_c) \tag{17}$$

where δ_p is the oil film thickness between the piston and the cylinder block, μ is the kinetic viscosity of the fluid, $l_{cp} = l_{cp0} + R(1 - \cos\varphi)\tan\gamma$ is the instantaneous overlap length of the piston and the cylinder block, l_{cp0} is the initial overlap length of the piston and the cylinder block when the piston is at the TDC, and P_c is the pressure of the pump shell chamber.

The leakage flow through the slipper and the swash plate is given by

$$Q_{lsi} = \frac{\pi d_{lh}^4 \delta_s^3}{\mu\left[6d_{lh}^4 \ln(R_s/r_s) + 128\delta_s^3 l_p\right]}(P_{pi} - P_c) \tag{18}$$

where d_{lh} is the diameter of the piston leakage hole, δ_s is the clearance between the slipper and the swash plate, R_s and r_s are the outer and the inner radii of the slipper, and l_p is the total length of the piston.

Another leakage flow depicted in Fig. 5 through the clearance between the cylinder block and the valve plate can be described in term of the variables shown in Fig. 2(a) as

$$Q_{lv} = \frac{\delta_v^3}{12\mu}\left[\frac{1}{\ln(R_2/R_1)} + \frac{1}{\ln(R_4/R_3)}\right](P_d - P_c) \tag{19}$$

where δ_v is the clearance between the valve plate and the cylinder block, R_1 and R_2 are the inside and outside radii of the inside value plate seal ring, and R_3 and R_4 are the inside and outside radii of the outside value plate seal ring as shown in Fig. 2(a).

3.2. Multi-piston model of the aviation axial-piston pump

The flow ripple of a multi-piston pump is due to the discontinuity in discharge flow rate from the piston and its governing pumping mechanism.[19] Therefore, the multi-piston model of the aviation axial-piston pump can be established by combining several single-piston models connecting to the discharge port, which are separated from each other by a phase angle equal to a separation angle of 360/9 degrees. The total flow generated by pistons connecting with the discharge port can be expressed as

$$Q_p = \sum_{i=1}^{5} Q_{pi}. \tag{20}$$

In addition, as the leakage flow through the gap between the cylinder block and the valve plate is the effect of multiple pistons, it should be added to the multi-piston pump model. Thus the pump's discharge flow into the discharge chamber is given by

$$Q_{pd} = Q_p - Q_{lv}. \tag{21}$$

The pressure pulsation, which results in noise propagating and pipe vibration, is affected not only by the flow ripple of

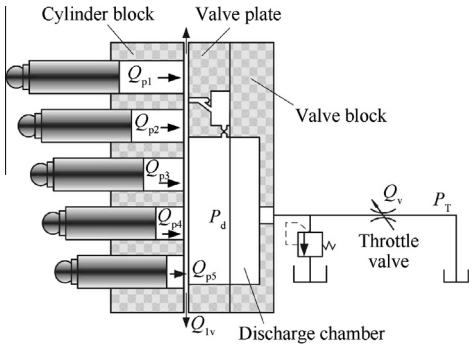

Fig. 6 Multi-piston model of the aviation pump with a simple hydraulic circuit.

the pump but also by the hydraulic system parameters. Conversely, the flow ripple is also affected by the pressure pulsation. Therefore, in order to establish the multi-piston model of the overall pump, the simple hydraulic system needs to be built by adding a throttle valve as the load, which is shown in Fig. 6.

The flow rate through the throttle valve is expressed by the classical orifice equation as

$$Q_v = C_v A_v \sqrt{\frac{2(P_d - P_t)}{\rho}} \tag{22}$$

where Q_v is the flow rate of the throttle valve, C_v is the discharge coefficient of the throttle valve, A_v is the discharge orifice area of the throttle valve, and P_t is the pressure of the tank.

In the discharge chamber, the continuity equation follows

$$\frac{dP_d}{dt} = \frac{E}{V_{dc}}(Q_{pd} - Q_v) \tag{23}$$

where V_{dc} is the control volume of the discharge chamber.

4. Computational technique

The equations in the developed single- and multi-piston models for the aviation axial-piston pump include first-order differential equations for pressure dynamics. A simultaneous solution of these differential and algebraic equations provides the pressure and flow characteristics of a single piston as well as the overall pump. The single- and multi-piston pump models are both solved using the 'S-function' in Matlab/Simulink environment.

Eqs. (2)–(18), which describe the single-piston model, are solved in one 'S-function'. The inputs of the 'S-function' are the time t and the pressure P_d in the discharge chamber. The state variables of the 'S-function' are the pressure P_{pi} in the piston chamber and the pressure P_{bc} in the buffer chamber. The output of the 'S-function' is the individual piston discharge flow Q_{pi}.

The differential Eq. (23) of the multi-piston pump model is solved by another 'S-function'. The inputs of this 'S-function' are the time t and the total flow Q_p generated by pistons which can be obtained by summarizing the outputs of each single piston's 'S-function'. The state variable and the output of the 'S-function' are both the pressure P_d in the discharge chamber.

5. Results and discussion

5.1. Validation of the model

In order to validate the developed multi-piston pump model, the computational fluid dynamic (CFD) technology, which is widely used to study the flow ripple of axial-piston pumps, is employed. The CFD model of an aviation axial-piston pump which consists of five pistons communicating with a discharge port, a linearized discharge port, and a pre-pressurization fluid path (a damping hole, a buffer chamber, and an orifice) is built as shown in Fig. 7.

The setting and solving of the CFD model is carried out in FLUENT V6.3. As shown in Fig. 7, there are two movements for pistons: the axial movement along its axial and the translational motion along the linearized discharge port. The axial movement is modeled by a dynamic grid with a moving mesh of the piston end face and a deforming mesh of the piston body. Meanwhile, the translational motion is realized by a sliding grid which provides the grid interface between the static linearized discharge port and the moving pistons. The two types of movements are both governed by a user-defined function (UDF) in FLUENT V6.3.

The fluid compressibility is considered in the CFD model by establishing the pressure-dependent density model based on the bulk modulus which is given by[23]

$$\rho_{ce} = \frac{\rho_0}{1 - (p_{ce} - p_0)/E} \tag{24}$$

where $\rho_0 = 900\ \mathrm{kg/m^3}$ is the reference density of the fluid at an ambient pressure of $p_0 = 0.101$ MPa, and p_{ce} is the pressure of the fluid cell in the grid. Eq. (24) is realized by a UDF in FLUENT V6.3.

In order to simplify the CFD model, the leakage flow rates are not taken into consideration, but this simplification does not affect the model validation because the equations of the leakage flow rates are classic. Meanwhile, in order to maintain the consistency with the CFD model, the leakage flows in the theoretical model are also ignored (only ignored in Section 5.1, but considered in Section 5.2). The simulation of the developed multi-piston model without leakage flows is carried out in Matlab V7.0. The simulation parameters are listed in Table 1 and the comparison of the simulation results by the CFD model and the theoretical model is shown in Fig. 8. From Fig. 8, reasonable agreement between the flow ripples from the two

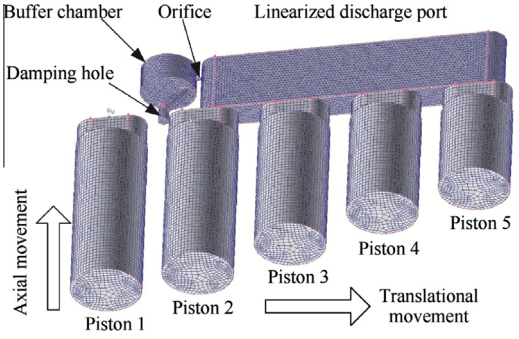

Fig. 7 CFD model of an aviation axial-piston pump with a linearized discharge port.

Table 1 Parametric values used in the simulation.

Symbol	Value	Symbol	Value	Symbol	Value
Z	9	μ	4.5×10^{-2} N.s/m^2	P_c	0 Pa
R	3.8×10^{-2} m	C_d	0.6	δ_p	5×10^{-5} m
n	3000 r/min	C_h	0.6	l_{cp0}	6×10^{-3} m
γ	$\pi/10$ rad	ρ	900 kg/m^3	δ_v	5×10^{-5} m
r_k	4.5×10^{-3} m	E	1×10^{9} Pa	d_{lh}	2×10^{-3} m
l_k	1.1×10^{-2} m	d_o	1×10^{-3} m	δ_s	5×10^{-5} m
d_h	3×10^{-3} m	α_1	$5\pi/180$ rad	R_s	2.59×10^{-2} m
V_0	1.57×10^{-5} m^3	α_2	$10\pi/180$ rad	r_s	3.6×10^{-3} m
d_p	2.05×10^{-2} m	α_3	$38\pi/180$ rad	l_p	6.8×10^{-2} m
l_{d1}	8×10^{-3} m	α_4	$43\pi/180$ rad	A_v	2.11×10^{-5} m^2
l_{d2}	6×10^{-3} m	β_1	$23\pi/180$ rad	V_{dc}	1×10^{-3} m^3
R_1	2.7×10^{-2} m	β_2	$36.5\pi/180$ rad	C_o	0.6
R_2	3.35×10^{-2} m	β_3	$53\pi/180$ rad	V_{bc}	4.0×10^{-6} m^3
R_3	4.25×10^{-2} m	β_4	$157\pi/180$ rad	P_T	0 Pa
R_4	5.7×10^{-2} m	β_5	π rad		

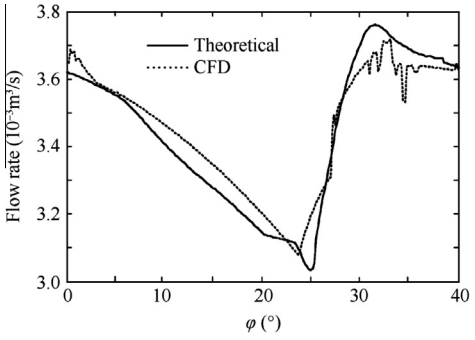

Fig. 8 Comparison of the aviation pump flow ripples from the theoretical model and the CFD model.

models is observed, so the accuracy of the developed multi-piston model for the aviation pump's flow ripple is acceptable.

5.2. *Effect of the pre-pressurization fluid path*

In order to examine the effect of the pre-pressurization fluid path on the flow ripple, the flow ripple of an axial-piston pump has been simulated by the proposed multi-piston model when changing the structural parameters of the pre-pressurization fluid path. It is worth noting that the multi-piston model applied in this section considers the leakage flows. The simulation parameters are listed in Table 1.

5.2.1. *With or without the pre-pressurization fluid path*

In order to examine the effect of the pre-pressurization fluid path in the valve plate, the flow ripple of the aviation axial-piston pump with the pre-pressurization fluid path is compared with that of the pump without the pre-pressurization fluid path in the valve plate. The flow ripple of the axial-piston pump without the pre-pressurization fluid path can also be calculated using the developed multi-piston pump model, but the damping hole, the buffer chamber, and the orifice shown in Fig. 2(a) cannot be considered. Fig. 9 depicts one cycle flow ripple of the aviation axial-piston pump with the two types of valve plates.

In Fig. 9, it is observed that the minimum and maximum values of the flow rate of the aviation axial-piston pump with

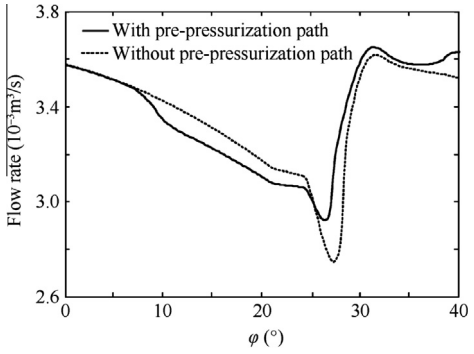

Fig. 9 One cycle flow ripple of the aviation axial-piston pump with or without the pre-pressurization fluid path.

and without the pre-pressurization fluid path are $(2.923\times10^{-3}$ m^3/s, 3.650×10^{-3} m^3/s) and $(2.747\times10^{-3}$ m^3/s, 3.617×10^{-3} m^3/s), respectively. It reveals that the flow ripple amplitude (0.727×10^{-3} m^3/s) of the aviation axial-piston pump with the pre-pressurization fluid path in the valve plate is lower than that (0.87×10^{-3} m^3/s) of the pump without the pre-pressurization fluid path.

The effect of the pre-pressurization fluid path on the instantaneous pressure in the piston chamber is also examined by the

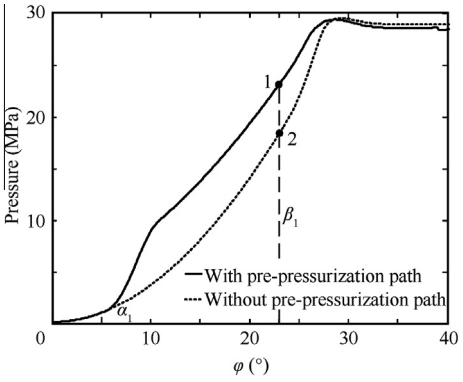

Fig. 10 Pressure in the piston chamber of the aviation axial-piston pump with or without the pre-pressurization fluid path.

single-piston model developed in Section 3.1. P_d = 28 MPa is set for the simulation of the single-piston model. Fig. 10 shows the instantaneous pressure in the piston chamber of the aviation axial-piston pump with or without the pre-pressurization fluid path in the valve plate. As shown in Fig. 10, the pressure in the piston chamber of the axial-piston pump with the pre-pressurization fluid path begins to rise more rapidly when the kidney port begins to communicate with the damping hole ($\varphi = \alpha_1$). When the piston kidney port communicates with the discharge port ($\varphi = \beta_1$), the pressure in the piston chamber of the pump with the pre-pressurization fluid path has risen to point 1 (23.84 MPa), while the pressure in the piston chamber of the pump without the pre-pressurization fluid path has risen to point 2 (19.35 MPa). It reveals that the pre-pressurization fluid path can reduce the pressure difference between the piston chamber and the discharge port which is the main factor of flow ripple in axial-piston pumps. This can explain why the flow ripple amplitude of the axial-piston pump with the pre-pressurization fluid path is lower than that of the pump without the pre-pressurization fluid path as shown in Fig. 9.

5.2.2. *Effect of the damping hole*

With reference to the modeling process of the single-piston model, the effect of the damping hole on the flow ripple of the aviation pump includes two factors: the diameter and the position of the damping hole. The two factors' effects on the flow ripple are examined.

5.2.2.1. Diameter of the damping hole. In order to examine the effect of the damping hole's diameter on the flow ripple, different diameters are adopted to the developed multi-piston model. The flow ripple curves of the aviation axial-piston pumps with different diameters of the damping hole are plotted in Fig. 11 and the flow ripple amplitudes are listed in Table 2.

From Fig. 11 and Table 2, we can see that: (a) the flow ripple amplitude decreases (from 0.8184×10^{-3} m^3/s to 0.6986×10^{-3} m^3/s) when the diameter of the damping hole increases (from 0.5 mm to 3.5 mm); (b) when the diameter of the damping hole increases from 3.5 mm to 5 mm, the change of the flow ripple amplitude (0.6986×10^{-3} m^3/s and 0.7001 m^3/s) is no longer significant. These can be explained by Fig. 12, which reveals that the pressure in the piston chamber rises when the diameter of the damping hole increases. This makes the pressure difference between the piston chamber and the discharge port when they begin to communicate at β_1 decrease, which reduces the inverse flow Q_d from the discharge port to the piston chamber. Meanwhile, when the diameter of the damping hole increases from 3.5 to 5 mm, the change of pressure in the piston chamber is no longer significant, which illustrates that 3.5 mm could be the optimal diameter.

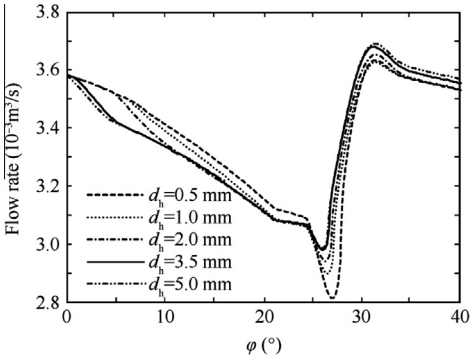

Fig. 11 Flow ripple curves of the aviation pump with different d_h.

5.2.2.2. Position of the damping hole. According to Fig. 4(a), the parameter α_1 represents the position of the damping hole. Thus in order to check the effect of the damping hole's position on the flow ripple, different α_1 are selected substituting to the developed multi-piston model. The flow ripple curves

Table 2 Flow ripples with different d_h, α_1, V_{bc}, and d_o.

Parameters	Values	Flow minimum (10^{-3} m^3/s)	Flow maximum (10^{-3} m^3/s)	Flow ripple amplitude (10^{-3} m^3/s)
d_h (mm)	0.5	2.8101	3.6285	0.8184
	1.0	2.8954	3.6223	0.7269
	2.0	2.9384	3.6476	0.7092
	3.5	2.9759	3.6745	0.6986
	5.0	2.9830	3.6831	0.7001
α_1 (°)	−5	2.9917	3.6714	0.6797
	−2	2.9849	3.6687	0.6838
	0	2.9787	3.6665	0.6878
	5	2.9225	3.6502	0.7277
	8	2.9042	3.6459	0.7417
V_{bc} (mL)	4	2.9225	3.6502	0.7277
	12	2.9189	3.6228	0.7039
	24	2.9616	3.5847	0.6231
	40	3.0184	3.5643	0.5459
	80	3.0747	3.4817	0.4070
d_o (mm)	2.5	2.9136	3.8030	0.8894
	2.0	2.9976	3.7739	0.7763
	1.5	3.0226	3.7008	0.6782
	1.0	2.9225	3.6502	0.7277
	0.5	2.8064	3.6275	0.8211

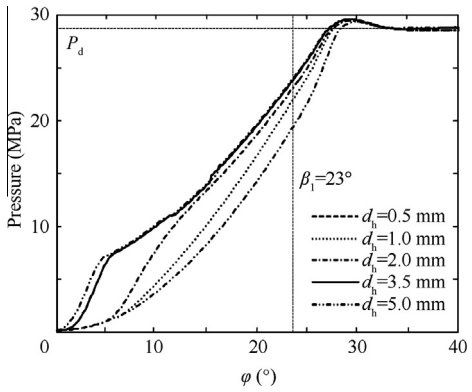

Fig. 12 Pressure in the piston chamber of the aviation pump with different d_h.

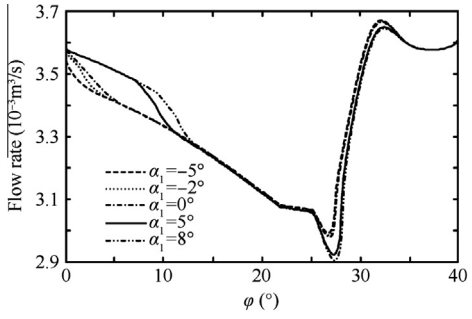

Figure 13 Flow ripple curves of the aviation pump with different α_1.

of the aviation axial-piston pump with different α_1 are plotted in Fig. 13 and the flow ripple amplitudes are listed in Table 2.

From Fig. 13 and Table 2, we can see that: (a) the flow ripple amplitude decreases (from 0.7417×10^{-3} m^3/s to 0.6797×10^{-3} m^3/s) when the damping hole moves towards to the TDC (from $\alpha_1 = 8°$ to $\alpha_1 = -5°$); (b) especially when α_1 is negative which represents that the piston kidney port intersects with the damping hole or includes the damping hole, the flow ripple amplitudes are significantly lower than those when α_1 is positive. These can be explained by Fig. 14, which reveals that the pressure in the piston chamber rises when the damping hole moves towards to the TDC. Especially when $\alpha_1 \leqslant 0$ ($\alpha_1 = 0°, -2°, -5°$), the pressure in the piston chamber begins to rise at $t = 0$ s. The rising of the pressure in the piston pump reduces the pressure difference between the piston chamber and the discharge port when they begin to communicate with each other at β_1. Therefore, the damping hole should be included in the piston kidney port when the piston kidney port is at the TDC in order to re-pressurize the fluid in the piston chamber more effectively.

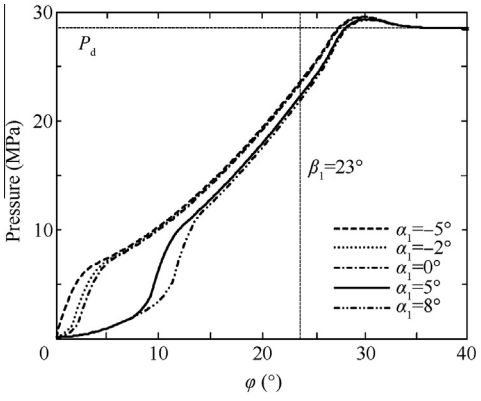

Fig. 14 Pressure in the piston chamber of the aviation pump with different α_1.

5.2.3. *Effect of the buffer chamber*

The buffer chamber shown in Fig. 2(a) is another component of the pre-pressurization fluid path. The effect of the buffer chamber on the flow ripple of the aviation axial-piston pump reflects in the volume of the buffer chamber, therefore the flow ripple of the aviation axial-piston pump with different V_{bc} is analyzed. The flow ripple curves of the aviation axial-piston pump with different V_{bc} are plotted in Fig. 15 and the flow ripple amplitudes are listed in Table 2.

With reference to Fig. 15 and Table 2, the flow ripple amplitude decreases (from 0.7277×10^{-3} m^3/s to 0.4070×10^{-3} m^3/s) when the volume of the buffer chamber increases (from 4 ml to 80 ml). This result can be explained clearly by Fig. 16. Fig. 16 shows that the pressure in the piston chamber rises when the

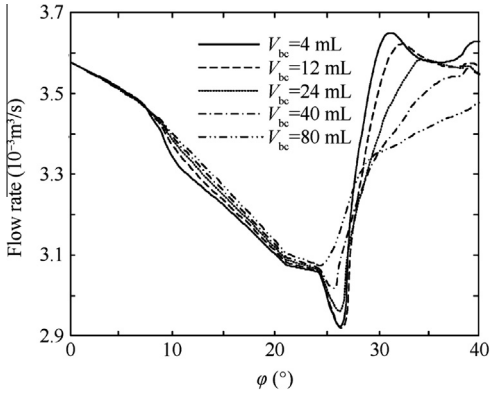

Fig. 15 Flow ripple curves of the aviation pump with different V_{bc}.

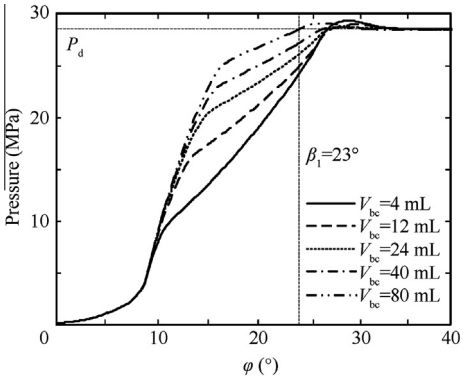

Fig. 16 Pressure in the piston chamber of the aviation pump with different V_{bc}.

volume of the buffer chamber increases from 4 to 80 ml. The rising of the pressure in the piston chamber reduces the pressure difference between the piston chamber and the discharge port when they begin to communicate with each other at β_1, which makes the inverse flow Q_d from the discharge port to the piston chamber smaller. Therefore, the buffer chamber should be designed to have a bigger volume in the allowable range of the valve plate to get a smaller flow ripple for the aviation axial-piston pump.

5.2.4. *Effect of the orifice*

The orifice between the buffer chamber and the discharge port shown in Fig. 2(a) is also a component of the pre-pressurization fluid path. The effect of the orifice on the flow ripple of the aviation axial-piston pump is examined by adopting different diameters of the orifice to the developed multi-piston model. The flow ripple curves are plotted in Fig. 17and the flow ripple values are listed in Table 2.

From Fig. 17 and Table 2, the flow ripple amplitude decreases (from $0.8211\times10^{-3}\,m^3/s$ to $0.6782\times10^{-3}\,m^3/s$) when the diameter of the orifice increases (from 0.5 to 1.5 mm), and then the flow ripple amplitude increases (from $0.6782\times10^{-3}\,m^3/s$ to $0.8894\times10^{-3}\,m^3/s$) when the diameter of the orifice increases (from 1.5 to 2.5 mm). This can be explained by Fig. 18. From Fig. 18, the minimum pressure difference between the piston chamber and the discharge port when they begin to communicate with each other at β_1 is observed when $d_o = 1.5$ mm. Therefore, $d_o = 1.5$ mm is the optimal value for the orifice in order to get the minimum flow ripple amplitude for the aviation axial-piston pump.

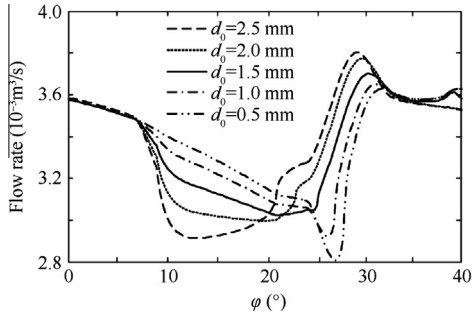

Fig. 17 Flow ripple curves of the aviation pump with different d_o.

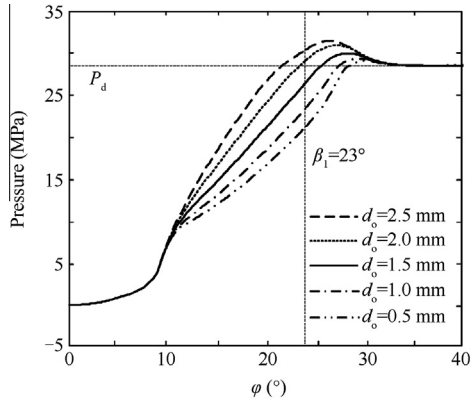

Fig. 18 Pressure in the piston chamber of the aviation pump with different d_o.

6. Conclusions

(1) A flow ripple model for an aviation axial-piston pump has been established which is validated by comparing with the CFD result. Compared with existing flow ripple models of an axial-piston pump with damping holes in the valve plate, the presented model is more comprehensive because it considers fluid compressibility, orifice restriction effect, fluid resistance in the capillary tube, and the leakage flow. This study enriches the flow ripple theory of axial-piston pumps.

(2) The single- and multi-piston models of the aviation axial-piston pump have been realized by the 'S function' in Matlab/Simulink environment. The computational technique has guiding significance to numerically analyze the flow ripple model of the axial-piston pump.

(3) The effects of the pre-pressurization fluid path on the flow ripple and the instantaneous pressure in the piston chamber have been studied. The pre-pressurization fluid path reduces the pressure difference between the piston chamber and the discharge port when they begin to communicate with each other, and this pressure difference results in the inverse flow which is the main cause of the flow ripple. Therefore, the design goal of the pre-pressurization fluid path is to minimize the pressure difference.

Acknowledgements

The authors gratefully acknowledge the support of the National Natural Science Foundation of China (No. 51235002) and the National Science Foundation for Distinguished Young Scholars (No. 50825502).

Appendix A. Derivation of A_{kh} at $[\alpha_1,\alpha_2]$

When the position angle is from α_1 to α_2, there will be two positional relationships between the kidney port and the damping hole, as shown in Fig. A1.

For the two positional relationships, the area of sector $ABEC$ can both be written by

$$A_{ABEC} = \frac{1}{2}\times\angle BAC\times r_h^2 = \theta_1 r_h^2 \tag{A1}$$

For Fig. A1(a):

The area of triangle ABC can be described as

$$A_{ABC} = \frac{1}{2}\times\overline{BC}\times\overline{AG} = \frac{1}{2}r_h^2\sin(2\theta_1). \tag{A2}$$

The area of arch BCE can be obtained by

$$A_{BCE} = A_{ABEC} - A_{ABC} = r_h^2\left(\theta_1 - \frac{1}{2}\sin(2\theta_1)\right). \tag{A3}$$

For Fig. A1(b):

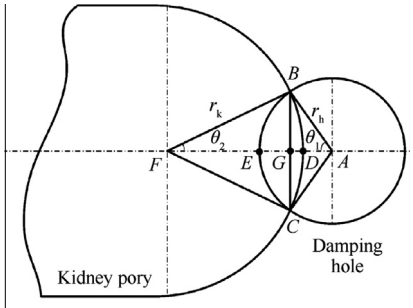

(a) θ_1<90°

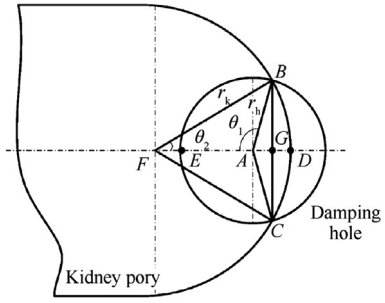

(b) θ_1>90°

Fig. A1 Two positional relationships between the kidney port and the damping hole at [α_1, α_2].

The area of triangle ABC can be expressed as

$$A_{ABC} = \frac{1}{2} \times \overline{BC} \times \overline{AG} = -\frac{1}{2} r_h^2 \sin(2\theta_1). \tag{A4}$$

The area of arch BCE can be written by

$$A_{BCE} = A_{ABEC} + A_{ABC} = r_h^2 \left(\theta_1 - \frac{1}{2} \sin(2\theta_1) \right). \tag{A5}$$

From Eqs. (A3) and (A5), we can see that the expressions for the areas of arch BCE of the two positional relationships are the same.

The following modeling for the two positional relationships is the same.

With reference to Eq. (A3), the area of arch BCD can be expressed as

$$A_{BCD} = A_{FBDC} - A_{FBC} = r_k^2 \left(\theta_2 - \frac{1}{2} \sin(2\theta_2) \right). \tag{A6}$$

Therefore, the discharge area A_{kh} at [α_1, α_2] can be derived as

$$\begin{aligned} A_{kh} &= A_{BCE} + A_{BCD} \\ &= r_h^2 \left(\theta_1 - \frac{1}{2} \sin(2\theta_1) \right) + r_k^2 \left(\theta_2 - \frac{1}{2} \sin(2\theta_2) \right). \end{aligned} \tag{A7}$$

Applying Law of cosines to triangle ABF yields

$$\cos\theta_1 = \frac{\overline{AB}^2 + \overline{AF}^2 - \overline{BF}^2}{2\overline{AB}\overline{AF}} \tag{A8}$$

$$\cos\theta_2 = \frac{\overline{BF}^2 + \overline{AF}^2 - \overline{AB}^2}{2\overline{BF}\overline{AF}} \tag{A9}$$

where

$$\overline{AF} = r_h + r_k - \overline{DE} = r_h + r_k - R(\varphi - \alpha_1). \tag{A10}$$

Combining Eqs. (A8)–(A10) yields

$$\theta_1 = \arccos \frac{r_h^2 + [r_h + r_k - (\varphi - \alpha_1)R]^2 - r_k^2}{2r_h[r_h + r_k - (\varphi - \alpha_1)R]} \tag{A11}$$

$$\theta_2 = \arccos \frac{r_k^2 + [r_h + r_k - (\varphi - \alpha_1)R]^2 - r_h^2}{2r_k[r_h + r_k - (\varphi - \alpha_1)R]}. \tag{A12}$$

Therefore, Eq. (A7) as well as Eqs. (A11) and (A12) describes the model of the discharge area A_{kh} when the position angle is at [α_1, α_2].

Appendix B. Derivation of A_{kh} at [α_3, α_4]

When the position angle is from α_3 to α_4, there will be two positional relationships between the kidney port and the damping hole, as shown in Fig. B1. The calculation of the discharge area A_{kh} in Fig. B1(a) is the same as that in Fig. A1(b), and the calculation of the discharge area A_{kh} in Fig. B1(b) is the same as that in Fig. A1(a). Therefore, the discharge area A_{kh} at [α_3, α_4] can be expressed as

$$A_{kh} = r_h^2 \left(\theta_3 - \frac{1}{2} \sin(2\theta_3) \right) + r_k^2 \left(\theta_4 - \frac{1}{2} \sin(2\theta_4) \right) \tag{B1}$$

where

$$\theta_3 = \arccos \frac{r_h^2 + [r_k + (\varphi - \alpha_3)R - r_h]^2 - r_k^2}{2r_h[r_k + (\varphi - \alpha_3)R - r_h]} \tag{B2}$$

$$\theta_4 = \arccos \frac{r_k^2 + [r_k + (\varphi - \alpha_3)R - r_h]^2 - r_h^2}{2r_k[r_k + (\varphi - \alpha_3)R - r_h]} \tag{B3}$$

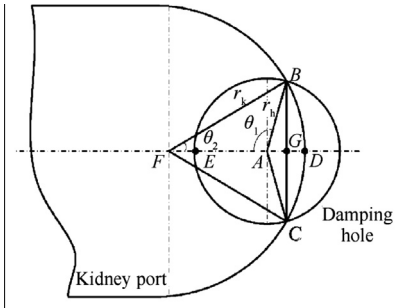

(a) θ_3>90°

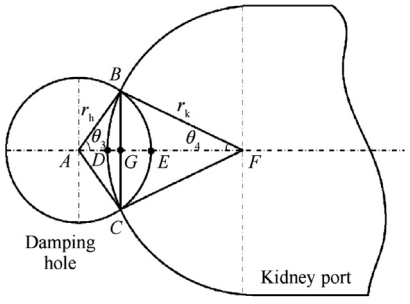

(b) θ_3<90°

Fig. B1 Two positional relationships between the kidney port and the damping hole at [α_3, α_4].

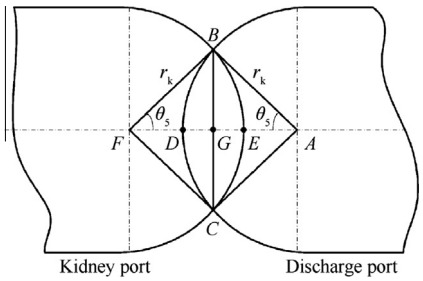

Fig. C1 The positional relationships between the kidney port and the discharge port at $[\beta_1, \beta_2]$.

Appendix C. Derivation of A_{kd} at $[\beta_1, \beta_2]$

The positional relationships between the kidney port and the discharge port at $[\beta_1, \beta_2]$ are shown in Fig. C1. The calculation of A_{kd} can refer to Fig. A1(a). Substituting $r_h = r_k$ into Eqs. (A7), (A11), and (A12) yields

$$A_{kd} = r_k^2(2\theta_5 - \sin(2\theta_5)) \tag{C1}$$

where

$$\theta_5 = \arccos\frac{2r_k - (\varphi - \beta_1)R}{2r_k} \tag{C2}$$

References

1. Wang ZM, Tan SK. Vibration and pressure fluctuation in a flexible hydraulic power systemon an aircraft. *Comput Fluids* 1998;**27**(1):1–9.
2. Cheah S. Design considerations of aircraft piping system. In: *Proceedings of the aerospace technological seminar*; 1993. p. 51–66.
3. Johansson A, Övander J, Palmberg JO. Experimental verification of cross-angle for noise reduction in hydraulic piston pumps. *Proc Inst Mech Eng I J Syst Control Eng* 2007;**221**(3):321–30.
4. Ma L. Theoretical analysis and experimental investigation of decreasing noise in swashplate axial piston pump. *Mach Tool Hydraul* 1987;**3**:19–25 [Chinese].
5. Qiu Z. Theoretical analysis and experimental investigation of the characteristics of noise reduction of damping structure in port plate for axial piston pump. *Mach Tool Hydraul* 1989;**5**:22–7 [Chinese].
6. Helgestad B, Foster K, Bannister F. Pressure transients in an axial piston hydraulic pump. *Proc Inst Mech Eng* 1974;**188**(1):189–99.
7. Edge K, Darling J. Cylinder pressure transients in oil hydraulic pumps with sliding plate valves. *Proc Inst Mech Eng B J Eng Manuf* 1986;**200**(1):45–54.
8. Edge K, Darling J. The pumping dynamics of swash plate piston pumps. *J Dyn Syst Meas Control* 1989;**111**:307–12.
9. Harrison K, Edge K. Reduction of axial piston pump pressure ripple. *Proc Inst Mech Eng I J Syst Control Eng* 2000;**214**(1):53–64.
10. Manring ND. The discharge flow ripple of an axial-piston swash-plate type hydrostatic pump. *J Dyn Syst Meas Control* 2000;**122**(2):263–8.
11. Manring ND. Valve-plate design for an axial piston pump operating at low displacements. *J Mech Des* 2003;**125**:200–7.
12. Manring ND, Zhang Y. The improved volumetric-efficiency of an axial-piston pump utilizing a trapped-volume design. *J Dyn Syst Meas Control* 2001;**123**(3):479–87.
13. Zhang X. New swash plate damping model for hydraulic axial-piston pump. *J Dyn Syst Meas Control* 2001;**123**:463–70.
14. Kassem S and Bahr M. Effect of port plate silencing grooves on performance of swash plate axial piston pumps. In: *Seventh conference on current advances in mechanical design and production*, 2000 Feb 15–17. Cairo, Egypt; 2000. p. 139–48.
15. Kassem S and Bahr M. On the dynamics of swash plate axial piston pumps with conical cylinder blocks. In: *Sixth triennial international symposium on fluid control measurement and visualization*. Sherbrooke, Canada; 2000. p. 13–7.
16. Bahr M, Svoboda J, Bhat R. Vibration analysis of constant power regulated swash plate axial piston pumps. *J Sound Vib* 2003;**259**(5):1225–36.
17. Khalil MKB. Modeling of swash plate axial piston pumps with conical cylinder blocks. *J Mech Des* 2004;**126**:196–202.
18. Li Z. *Condition monitoring of axial piston pump [dissertation]*. Saskatoon: University of Saskatchewan; 2005.
19. Ma J, Fang Y, Xu B, Yang H. Optimization of cross angle based on the pumping dynamics model. *J Zhejiang Univ Sci A* 2010;**11**(3):181–90.
20. Mandal N, Saha R, Sanyal D. Theoretical simulation of ripples for different leading-side groove volumes on manifolds in fixed-displacement axial-piston pump. *Proc Inst Mech Eng I J Syst Control Eng* 2008;**222**(6):557–70.
21. Bergada J, Kumar S, Davies DL, Watton J. A complete analysis of axial piston pump leakage and output flow ripples. *Appl Math Model* 2011;**36**(4):1731–51.
22. Jaroslav I, Monika I. *Hydrostatic pumps and motors*. New Delhi, India: Academia Book International; 2001.
23. Ma JE, Xu B, Zhang B, Yang HY. Flow ripple of axial piston pump with computational fluid dynamic simulation using compressible hydraulic oil. *Chin J Mech Eng* 2010;**23**(1):45–52.

Guan Changbin received his B.S. degree from China University of Petroleum in 2007 and now is a Ph.D. candidate in the school of automatic science and electric engineering at Beihang University. His main research interests include mechanical-electrical-hydraulic system modeling and simulation, smart hydraulic components and active control of fluid pulsation.

Jiao Zongxia is a professor and Ph.D. advisor in the school of automatic science and electric engineering at Beihang University. He received his Ph.D. degree from Zhejiang University in 1991. His current research interests are fluid power transmission and control, mechatronics systems and simulation engineering.

He Shouzhan is an M.S. student in the school of automatic science and electric engineering at Beihang University. He received his B.S. degree from Wuhan University of Technology in 2010. His area of research is passive control of fluid pulsation.